

# Toward Operationalizing Rasmussen: Drift Observability on the Simplex for Evolving Systems

Anatoly A. Krasnovsky

Department of Computer Science and Engineering  
Innopolis University  
Innopolis, Russia  
MB3R Lab  
Innopolis, Russia

## Abstract

Monitoring *drift into failure* is hindered by Euclidean anomaly detection that can conflate safe operational trade-offs with risk accumulation in signals expressed as *shares*, and by architectural churn that makes fixed schemas (and learned models) stale before rare boundary events occur. Rasmussen’s dynamic safety model motivates drift under competing pressures, but operationalizing it for software is difficult because many high-value operational signals (effort, remaining margin, incident impact) are *compositional* and their parts evolve. We propose a vision for *drift observability on the simplex*: model drift and boundary proximity in Aitchison geometry to obtain coordinate-invariant direction and distance-to-safety in interpretable balance coordinates. To remain comparable under churn, a monitor would continuously refresh its part inventory and policy-defined boundaries from engineering artifacts and apply lineage-aware aggregation. We outline early-warning diagnostics and falsifiable hypotheses for future evaluation.

## Keywords

Site Reliability Engineering, Drift into Failure, Compositional Data Analysis, Observability, Microservices

## 1 Motivation: Drift requires a dynamic state

Rasmussen’s “dynamic safety model” frames safety as a moving target: systems operate under competing gradients (e.g., efficiency vs. thoroughness), and local adaptations can produce a slow *drift toward failure* when boundaries of safe operation are approached[11, 22, 27]. Related safety and resilience traditions emphasize the same core challenge: accidents are emergent phenomena in sociotechnical systems, and they are rarely explained by a single broken component[12, 17, 19].

Software operations is a natural target: services evolve continuously, are governed by explicit policies (SLOs, error budgets), and emit rich telemetry. But teams reason about multi-objective state that is naturally *compositional*—shares of effort, remaining margin, or incident impact across parts. Such share signals live on the simplex and require log-ratio geometry to avoid closure artifacts[1, 25, 31]; Sec. 3.4 illustrates a concrete Euclidean pitfall. Equally important, the relevant parts evolve (splits/merges, request classes, SLO revisions), so a hand-maintained state vector quickly becomes stale.

**Scope.** In software operations, many relevant boundaries are explicit *policies* (SLO targets, error budgets, toil budgets), unlike the

often-invisible safety boundaries in Rasmussen’s original case studies. This paper focuses on policy-defined boundaries as a pragmatic starting point for drift observability; discovering unknown or disputed boundaries remains complementary work (e.g., post-incident learning, resilience testing).

**Thesis.** Drift monitoring in software operations needs a state representation that is geometry-correct for compositional signals and stable under architectural change. We propose modeling the operating point as a simplex composition analyzed in Aitchison geometry, and keeping it aligned with the running system by continuously refreshing part inventories and policy-defined boundaries from artifacts and stabilizing them via lineage-aware aggregation.

**Contributions.** (1) Rasmussen-style drift observability on the simplex: Aitchison-geometry drift direction and distance-to-safety in balance space. (2) Stabilization under churn via part lineage and aggregation to canonical groups. (3) A sketch of how artifact-derived inventories and policy-defined boundaries (automatic where available, otherwise bootstrapped) can supply the inputs needed for implementation and evaluation.

## 2 Preliminaries

### 2.1 Compositions and Aitchison geometry

A (strictly positive) composition with  $D$  parts is a vector  $\mathbf{x} \in \mathcal{S}^{D-1} = \{\mathbf{x} \in \mathbb{R}_{>0}^D : \sum_i x_i = 1\}$ . The appropriate geometry on the simplex is Aitchison geometry, where the key operations are *perturbation*  $\mathbf{x} \oplus \mathbf{y} = C(x_1 y_1, \dots, x_D y_D)$  and *powering*  $\alpha \odot \mathbf{x} = C(x_1^\alpha, \dots, x_D^\alpha)$ , with  $C(\cdot)$  normalizing to sum to one[1, 15]. Log-ratio coordinates map the simplex isometrically to Euclidean space. In particular, an isometric log-ratio (ilr) transform maps  $\mathcal{S}^{D-1}$  to  $\mathbb{R}^{D-1}$ , and its coordinates correspond to orthogonal *balances* (log-contrasts) between groups of parts[14, 15].

### 2.2 Artifact-derived operational models

We use *artifact-grounded model inference*: extracting a lightweight, analyzable model of a running system from artifacts such as deployment/configuration specs, SLO definitions, and traces. In microservice settings, distributed tracing provides an empirical call graph and latency structure[18, 24, 29]; deployments (e.g., Kubernetes manifests) encode intended structure and constraints[30]; and SLO-as-code (e.g., OpenSLO) yields machine-checkable reliability policies[23]. Surveys report that observability data and models are central to operating microservices at scale[20].

### 3 Drift observability on the simplex

#### 3.1 From models to compositional state

Let  $\mathcal{A}_t$  denote the artifact/telemetry stream at time  $t$  (traces, metrics, SLO-as-code, deployment specs, change events). An extraction operator yields a lightweight model  $\mathcal{M}_t = \text{Extract}(\mathcal{A}_t)$  (e.g., a dependency graph, an SLO inventory, a request-class partition)[23, 24, 29]. We only require that  $\mathcal{M}_t$  provides (i) a current part inventory with lineage/aggregation structure and (ii) policy-defined boundaries in a machine-checkable form where available; otherwise, a small seed set can be bootstrapped (e.g., from alert rules) before automation.

We then define the compositional operating point as a *model-induced composition*

$$\mathbf{x}_t = C(\Phi(\mathcal{M}_t, \mathcal{A}_t)) \in \mathcal{S}^{D(t)-1}, \quad (1)$$

where  $\Phi$  maps artifacts into a positive vector of “parts” and  $D(t)$  is allowed to change. Automated extraction can reduce manual burden: the model supplies the current set of parts, their aggregation structure, and the boundaries that define “unsafe” regions.

*Examples of model-induced compositions.* *Effort composition.*  $x_{t,i}$  is the share of engineering time spent on an operational work category (feature delivery, reliability engineering, toil). Effort shares require an explicit measurement protocol (e.g., issue/PR labeling and time accounting) and are used here mainly for intuition; empirical studies can start with telemetry-derived compositions such as SLO margin shares.

*Margin composition.*  $x_{t,i}$  is the share of remaining error budget across SLOs (or user journeys). *Risk/impact composition.*  $x_{t,i}$  is the share of expected incident impact attributed to service  $i$ , where attributions are computed by graph-based what-if analysis (simulation and/or targeted fault injection) on a dependency graph[2, 16].

*Evolving parts via model-based balances.* ilr coordinates are not unique, and interpretability depends on how parts are grouped into balances. Sequential binary partitions are therefore a design choice: in microservice settings, plausible hierarchies (criticality tiers, architectural layers, ownership) can conflict. We propose to derive a small set of candidate partitions from artifact-derived structure (e.g., SLO tiers and service-graph communities) and either (i) fix one as the operational view, or (ii) report sensitivity of drift attribution across candidates. In all cases, we define balances primarily over the *canonical groups* maintained by lineage ( $\pi_t$  below), so drift remains comparable across time at the coarse level; within-group partitions can be enabled once a group stabilizes[14].

*Part lineage and stable coordinates under  $D(t)$  changes.* When  $D(t)$  changes (service split/merge, renames, SLO revisions), raw ilr coordinates are not directly comparable across time. We maintain a lineage map  $\pi_t : \{1, \dots, D(t)\} \rightarrow \{1, \dots, K\}$  from current parts to a small, stable set of canonical groups (e.g., user journeys  $\rightarrow$  tiers  $\rightarrow$  service layers), and monitor the amalgamated state  $\tilde{\mathbf{x}}_t \in \mathcal{S}^{K-1}$  with  $\tilde{x}_{t,k} = \sum_{i:\pi_t(i)=k} x_{t,i}$ . We keep  $K$  small (typically 3–7) and use leaf-level  $\mathbf{x}_t$  only for drill-down within stable groups; low-confidence or short-lived parts go to an explicit “other” group. Because  $\mathcal{M}_t$  is inferred, alarms are gated by extraction confidence  $c_t$ , and large mass in “other” ( $m_t^{\text{other}} = \tilde{x}_{t,\text{other}}$ ) triggers re-baselining or model refinement. To reduce gaps inside “other”, surface its largest contributors and flag fast-growing newcomers.

**Lineage events.** In practice,  $\pi_t$  can be updated from artifacts with simple rules: renames preserve the canonical group id; splits and merges stay within a group to keep  $\tilde{\mathbf{x}}_t$  continuous; new parts route to “other” until ownership and policy surface are stable.

#### 3.2 Dynamics on the simplex under pressure

Following Rasmussen, we separate the compositional operating point from external “pressures” that bias how effort, margin, or risk is redistributed across parts. To avoid ill-typed operations under changing part inventories, we write the state equation on the fixed-size monitoring state  $\tilde{\mathbf{x}}_t \in \mathcal{S}^{K-1}$  over canonical groups (Sec. 3.1); finer leaf-level dynamics can be handled analogously within a stable group after re-closure.

We model one-step drift as

$$\tilde{\mathbf{x}}_{t+1} = \tilde{\mathbf{x}}_t \oplus (\beta \odot \tilde{\mathbf{g}}_t) \oplus \tilde{\boldsymbol{\eta}}_t, \quad (2)$$

where  $\tilde{\mathbf{g}}_t \in \mathcal{S}^{K-1}$  is an *effective pressure* over canonical groups,  $\beta \geq 0$  is a step size, and  $\tilde{\boldsymbol{\eta}}_t$  captures multiplicative noise. When pressure proxies are available at finer granularity, they can be aggregated into  $\tilde{\mathbf{g}}_t$  (e.g., by within-group (weighted) geometric means) before closure. Implementations should compute powering in log space and clamp tiny components to avoid numerical underflow.

In ilr coordinates  $\tilde{\mathbf{z}}_t = \text{ilr}(\tilde{\mathbf{x}}_t)$ , Eq. (2) corresponds to an additive state equation in Euclidean space:  $\tilde{\mathbf{z}}_{t+1} = \tilde{\mathbf{z}}_t + \beta \tilde{\mathbf{u}}_t + \boldsymbol{\epsilon}_t$  with  $\tilde{\mathbf{u}}_t = \text{ilr}(\tilde{\mathbf{g}}_t)$ . In practice, only the product  $\beta \tilde{\mathbf{u}}_t$  is identifiable from observed state changes, so we treat the normalized drift direction  $\hat{\mathbf{u}}_t = \Delta \tilde{\mathbf{z}}_t / \|\Delta \tilde{\mathbf{z}}_t\|$  as the primary directional signal and interpret  $\beta$  as the forecast horizon/step size. We make no strong distributional assumption on  $\boldsymbol{\epsilon}_t$ ; robust smoothing in ilr space suffices for early-warning diagnostics, while Gaussian state-space models are an optional approximation[1, 25].

**Interpreting pressure.** Rasmussen’s competing gradients are multi-dimensional; our  $\tilde{\mathbf{g}}_t$  should be read as an *effective relative pressure* that redistributes a fixed resource budget across parts (a natural assumption for effort and margin shares). Relaxing this to multiple independent pressure magnitudes and mapping them to simplex perturbations is an important direction for future work.

**Estimating drift direction.** Even when  $\tilde{\mathbf{g}}_t$  is not directly observed, the drift direction can be estimated in balance space by smoothing  $\Delta \tilde{\mathbf{z}}_t = \tilde{\mathbf{z}}_{t+1} - \tilde{\mathbf{z}}_t$  (e.g., robust EWMA or a state-space model) and reporting the dominant balance components. Because balances are orthogonal, this yields a sparse, interpretable summary of which trade-offs are moving.

#### 3.3 Boundary proximity and early warnings

In the simplex view, “approaching a boundary” often means that one or more parts become small: there is little remaining share of time, margin, or redundancy for some objective. We highlight two basic, geometry-correct diagnostics, and then generalize them to explicit policy constraints.

**Which state do we monitor?** To keep signals comparable under split/merge churn, we define global diagnostics on the stabilized monitoring state  $\tilde{\mathbf{x}}_t \in \mathcal{S}^{K-1}$  (Sec. 3.1). When a canonical group is stable and finer granularity is needed, the same formulas can be applied within that group on a re-closed subcomposition of the leaf-level state.

**Barrier index.**  $B(\tilde{x}_t) = -\sum_{k=1}^K \log \tilde{x}_{t,k}$ , which diverges as any  $\tilde{x}_{t,k} \rightarrow 0$ . This captures “distance from collapse” when boundaries correspond to near-zero shares.

**Distance to a safe reference.** For a reference composition  $\tilde{x}^*$  (chosen by experts or learned as the Aitchison mean of a historically “known-good” window), the Aitchison distance is  $d_A(\tilde{x}_t, \tilde{x}^*) = \|\text{ilr}(\tilde{x}_t) - \text{ilr}(\tilde{x}^*)\|_2$ . Unlike Euclidean distance on raw shares,  $d_A$  is invariant to multiplicative rescaling and admits a directional interpretation: dominant components of  $\text{ilr}(\tilde{x}_t) - \text{ilr}(\tilde{x}^*)$  identify the balances (trade-offs) that are drifting.

**Choosing and updating  $\tilde{x}^*$ .** For cold-start, a monitor can remain in a “learning mode” until it has enough history to estimate a stable baseline (e.g., several weeks of daily samples), suppressing distance-based alerts. To adapt to benign evolution while still detecting drift,  $\tilde{x}^*$  can be updated slowly in ilr space (e.g., exponential smoothing) and *frozen* during major interventions (incident response, error-budget gates, large migrations) or when model health degrades (low extraction confidence  $c_t$ , high mass in “other”  $m_t^{\text{other}}$ ).

**Policy barriers beyond near-zero shares.** Operational boundaries are often expressed as inequality constraints  $h_j(\mathbf{x}) \leq 0$  (toil caps, concentration limits, error-budget gates). To remain coordinate-invariant, ratio constraints should be encoded as *log-ratios*; for example, the safety boundary  $F/R \leq \tau$  is  $h(\mathbf{x}) = \log(F/R) - \log \tau$  (rather than  $F - \tau R$ ). For a safe set  $\Omega = \{\mathbf{x} \in S^{K-1} : h_j(\mathbf{x}) < 0 \forall j\}$ , a generic log-barrier is  $B_\Omega(\mathbf{x}) = -\sum_i \log x_i - \sum_j \log(-h_j(\mathbf{x}))$ , which diverges as any constraint is approached. A complementary diagnostic is the *step-to-boundary* along the estimated drift direction in ilr space: let  $\tilde{z}_t = \text{ilr}(\tilde{x}_t)$  and  $\hat{u}_t$  be the (smoothed) drift direction; then we seek the smallest  $\lambda > 0$  such that  $\text{ilr}^{-1}(\tilde{z}_t + \lambda \hat{u}_t) \notin \Omega$ . In practice, this is a 1D root-finding problem (e.g., bisection on  $\lambda \in [0, \lambda_{\max}]$  with tolerance  $\epsilon$ ); if no constraint is reached within  $\lambda_{\max}$ , report  $\lambda > \lambda_{\max}$  (boundary distant), and if the direction points strictly inward, report  $\lambda = \infty$ .

### 3.4 The Euclidean pitfall: conflated trade-offs

Because compositions are constrained to sum to one, independent trends in raw components can be misleading. Figure 1 provides a minimal example on the weekly effort composition  $\mathbf{x}_t = (F_t, R_t, O_t)$  for feature work, reliability work, and operations/toil. In both panels, the black point ( $t_0$ ) is the same baseline  $\mathbf{x}^{(0)}$  with  $F/R = 1.00$ . The two panels then illustrate two qualitatively different one-step changes:

(A) *Euclidean illusion (false positive)*. The move to  $\mathbf{x}^{(C)}$  reduces  $O$  and (by closure) increases both  $F$  and  $R$  while keeping  $F/R$  unchanged ( $t_1$  remains on the green  $F = R$  line). A Euclidean threshold around  $\mathbf{x}^{(0)}$  can fire even though the feature-reliability trade-off did not change.

(B) *Euclidean blind spot (false negative)*. The move to  $\mathbf{x}^{(B)}$  stays within the same Euclidean threshold but increases the ratio to  $F/R \approx 1.96$ , crossing the illustrative safety boundary  $F > 1.5R$ .

One concrete instantiation consistent with the stacked bars in Fig. 1 is  $\mathbf{x}^{(0)} \approx (0.33, 0.33, 0.34)$ ,  $\mathbf{x}^{(C)} \approx (0.44, 0.44, 0.12)$ , and  $\mathbf{x}^{(B)} \approx (0.45, 0.23, 0.32)$ . In balance coordinates for the sequential partition ( $F$  vs.  $R$ ) and ( $\{F, R\}$  vs.  $O$ ), the first balance is  $\frac{1}{\sqrt{2}} \log(F/R)$ : it changes for  $\mathbf{x}^{(B)}$  (from 0 to  $\approx 0.48$ ) but not for  $\mathbf{x}^{(C)}$ . Conversely,

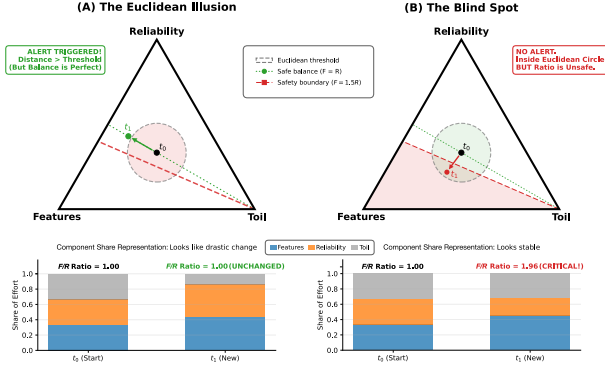


**Figure 1: Effort shares  $\mathbf{x} = (F, R, O)$  on the simplex (F feature, R reliability, O toil). Baseline  $t_0 \rightarrow t_1$ : (A) Euclidean alarm although  $F/R$  is unchanged; (B) no alarm although  $F/R > 1.5$  (unsafe). Dashed circle: Euclidean threshold; green:  $F = R$ ; red:  $F = 1.5R$ .**

the second balance  $\sqrt{\frac{2}{3}} \log(\sqrt{F}R/O)$  changes strongly for  $\mathbf{x}^{(C)}$  (toil shrinks) but is near-constant for  $\mathbf{x}^{(B)}$ . Figure 1 visualizes these (approximately) orthogonal directions on the effort-share simplex. This is the core benefit of working in log-ratio coordinates: drift is localized to interpretable trade-offs rather than conflated across constrained shares[14, 31].

### 3.5 From drift metrics to operational action

To be useful, drift observability must map geometric signals to decisions. We envision a monitor that, at each time step, emits a compact *drift report*: (1) a scalar warning level from  $d_A(\tilde{x}_t, \tilde{x}^*)$  and its trend; (2) an *imminence* estimate via step-to-boundary along the estimated drift direction; (3) *attribution* via the top- $k$  balances contributing to  $\text{ilr}(\tilde{x}_t) - \text{ilr}(\tilde{x}^*)$ , mapped back to model structure via the partition derived from  $\mathcal{M}_t$ ; and (4) *model-health* indicators (extraction confidence  $c_t$ , mass in “other”  $m_t^{\text{other}}$ ). This report can drive actions already common in SRE: pausing releases when the estimated step-to-boundary is small (i.e., boundary imminence is high), allocating reliability work when the  $F/R$  balance drifts, focusing investigation when risk concentrates in a single tier, and triggering re-instrumentation or re-baselining when  $c_t$  drops or  $m_t^{\text{other}}$  grows. Operators need not see log-ratio coordinates: the UI can surface labeled trade-off indicators.

## 4 Running example

Site Reliability Engineering (SRE) offers explicit operational boundaries and artifacts. SLOs define reliability targets, error budgets quantify allowable unreliability, and teams use these signals to trade feature velocity against reliability work[3–5]. SRE guidance also aims to cap operational work (toil) to preserve engineering capacity[6, 7]. This setting naturally produces model-induced compositions.

## 4.1 Artifact-derived parts and boundaries

**SLO margin composition.** Automated model extraction can parse an SLO-as-code repository (e.g., OpenSLO) to obtain the current set of SLOs and their error budgets[23]. Let  $u_{t,i}$  be remaining error budget (or remaining headroom) for SLO  $i$ ; then  $\mathbf{x}_t = C(u_{t,1}, \dots, u_{t,D})$  is a composition over SLOs. Boundaries correspond to one or more  $u_{t,i} \rightarrow 0$ . If an SLO is already over budget ( $u_{t,i} < 0$ ), treat this as a boundary violation and keep the closed composition positive (e.g., by clamping to  $\epsilon$ ) while tracking deficit magnitude separately.

**Risk-share composition from dependency graphs.** Model extraction from traces and deployment data can produce a service graph and a set of user journeys[20, 29, 30]. Graph simulation then provides a scalable estimate of how risk or impact is distributed across services, yielding a “risk-share” composition that can be monitored for concentration[2, 16]. This creates a direct bridge between drift monitoring and chaos engineering: fault injection acts as an exogenous pressure shock, and drift metrics become outcome variables.

## 4.2 Toy drift scenarios (illustrative only)

To connect to Rasmussen’s intuition, we reuse the effort-share composition  $\mathbf{x}_t = (F_t, R_t, O_t) \in \mathcal{S}^2$  and the two one-step scenarios in Fig. 1. Assume an organization encodes an illustrative policy such as  $F/R \leq 1.5$  (feature work should not exceed reliability by more than 50%) and treats the baseline  $\mathbf{x}^{(0)}$  as “known-good.” Panel (A) is a benign efficiency shift:  $O$  shrinks and the raw shares of  $F$  and  $R$  increase by closure, but the critical balance  $F/R$  is unchanged. Panel (B) is a risky shift:  $F/R$  increases and crosses the boundary while remaining Euclidean-near to the baseline. A drift monitor built on log-ratio coordinates would therefore emphasize balance-specific signals (e.g., the  $F/R$  balance and the step-to-boundary along  $\hat{\mathbf{u}}_t$ ), not just share-wise changes. This example is illustrative; empirical studies would instantiate  $\mathbf{x}_t$  from artifacts/telemetry (Sec. 3.1) and validate lead time before real boundary events.

## 5 Research agenda and evaluation design

As a vision paper, we focus on a testable framing and outline falsifiable outcomes rather than a full empirical study.

### 5.1 Operationalization tasks

**Discover parts and boundaries.** Use SLO-as-code, traces, and deployment artifacts to keep an up-to-date inventory of parts and safety boundaries[23, 24, 30]. **Map telemetry to positive parts.** Define  $\Phi(\mathcal{M}_t, \mathcal{A}_t)$  for each use case (effort, margin, risk/impact); graph-based what-if analysis and fault-injection experiments are one concrete path for risk attribution[2, 16]. **Handle zeros coherently.** Operational data contains rounded zeros (below measurement resolution), structural zeros (true absence), and missingness (instrumentation gaps). CoDA requires principled treatment: multiplicative replacement for rounded zeros, explicit confidence gating for missingness, and keeping “deficits” (e.g., negative remaining budget) as boundary violations rather than negative parts in a closed composition[21]. **Choose interpretable balances.** Derive sequential binary partitions from the extracted model (e.g., service layers, critical vs. non-critical journeys) so drift directions correspond to actionable trade-offs[14]. **Stabilize under model**

**evolution.** Track part lineage across splits, merges, or renames, and project to a stable set of canonical groups (Sec. 3.1) so drift is comparable under churn; treat major instrumentation changes (e.g., tracing sampling shifts) as confounders that trigger re-baselining rather than “true” drift; track extraction confidence  $c_t$  and mass in “other”  $m_t^{\text{other}}$  to gate alarms and request re-baselining/model refinement when model health degrades.

## 5.2 Hypotheses

**H1 (directional drift).** During sustained exogenous shocks (magnitude  $> 1\sigma$  above baseline, duration  $\geq L$  consecutive windows), the smoothed drift in balance space  $\Delta\tilde{\mathbf{z}}_t$  exhibits a non-zero mean direction after controlling for seasonality; operationally,  $\|\mathbb{E}[\Delta\tilde{\mathbf{z}}_t]\|_2$  exceeds a high quantile of the pre-shock drift-norm distribution. **H2 (early warning).** In a pre-event window of length  $W$ , the barrier index  $B(\tilde{\mathbf{x}}_t)$  or the distance  $d_A(\tilde{\mathbf{x}}_t, \tilde{\mathbf{x}}^*)$  shows a statistically significant upward trend (e.g., monotone-trend or slope tests), yielding a practically meaningful median lead time  $\geq \ell_{\min}$  before boundary events. **H3 (localization).** Drift energy concentrates in a small number of balances: letting  $E_j = \sum_t (\Delta\tilde{z}_{t,j})^2$ , the top  $k$  balances (largest  $E_j$ ) explain at least  $p\%$  of  $\sum_j E_j$  for small  $k$  (e.g.,  $k \leq 3$ ), and outperform random-partition baselines.

## 5.3 Evaluation sketches

**Quasi-experimental shocks.** Use policy changes (introducing an error-budget gate), reorganizations, or planned chaos experiments as exogenous shifts in  $\mathbf{g}_t$  (or  $\mathbf{u}_t$  in balance space)[2, 16].

**Baselines.** Compare against (i) standard SRE signals and alerting rules (e.g., error-budget depletion/burn-rate alerts), (ii) univariate change detection on raw shares, (iii) pairwise log-ratio monitoring without full CoDA geometry, and (iv) Euclidean analyses of raw shares (component-wise trends, Euclidean distance to a reference), to test whether Aitchison-geometry diagnostics provide earlier or less noisy warnings.

**Synthetic stress tests for part churn.** Generate synthetic drift trajectories with explicit split/merge and renaming events, and compare false-positive/false-negative rates with and without lineage-aware aggregation (Sec. 3.1).

**Synthetic benchmarks for drift + attribution.** Construct a simple generator in ilr space: sample  $\mathbf{z}_t$  from a linear state model with piecewise-constant drift vectors, map back to  $\mathbf{x}_t$  via  $\text{ilr}^{-1}$ , and inject split/merge events through  $\pi_t$ . This supports quantitative criteria even with synthetic data: (a) detection delay to boundary crossings, (b) false-alarm rates under stationary regimes, and (c) attribution fidelity—whether the top- $k$  reported balances match the injected drift direction.

**Validity.** Assess robustness to instrumentation drift and whether artifact-derived models reduce manual measurement effort.

## 6 Positioning and related work

This vision links safety-science drift models[11, 12, 22, 27], compositional data analysis[1, 14, 15, 25, 31], and artifact-derived observability and dependability analysis for distributed systems[2, 16, 18, 20, 29, 30]. In software engineering, CoDA has been used for cumulative voting and effort-phase distributions[8–10, 28]. We contribute a geometry-correct drift monitor on the simplex, stabilized

under churn via lineage-based aggregation, with artifact-derived models bridging artifacts to state.

## 7 Conclusion

Rasmussen's model suggests drift arises from local optimization under competing pressures. We propose drift observability for evolving software systems: monitor compositional state in Aitchison geometry and stabilize it under churn via lineage-based aggregation to canonical groups, with artifact-derived models keeping parts and policy boundaries current and gating alerts via model health (confidence, mass in "other"). Future work extends this approach to distribution-valued telemetry (e.g., latency histograms) using Bayes Hilbert spaces [13, 26].

## References

- [1] John Aitchison. 1986. *The Statistical Analysis of Compositional Data*. Chapman & Hall.
- [2] Ali Basiri, Niosha Behnam, Ruud de Rooij, Lorin Hochstein, Luke Kosewski, Justin Reynolds, and Casey Rosenthal. 2016. Chaos Engineering. *IEEE Software* 33, 3 (2016), 35–41. [doi:10.1109/MS.2016.60](https://doi.org/10.1109/MS.2016.60)
- [3] Betsy Beyer, Chris Jones, Jennifer Petoff, and Niall Richard Murphy. 2016. Embracing Risk. Online chapter in *Site Reliability Engineering*. <https://sre.google/sre-book/embracing-risk/> Accessed 2026-01-20.
- [4] Betsy Beyer, Chris Jones, Jennifer Petoff, and Niall Richard Murphy. 2016. Service Level Objectives. Online chapter in *Site Reliability Engineering*. <https://sre.google/sre-book/service-level-objectives/> Accessed 2026-01-20.
- [5] Betsy Beyer, Chris Jones, Jennifer Petoff, and Niall Richard Murphy. 2016. *Site Reliability Engineering: How Google Runs Production Systems*. O'Reilly Media.
- [6] Betsy Beyer, Niall Richard Murphy, David K. Rensin, Kent Kawahara, and Stephen Thorne. 2018. Eliminating Toil. Online chapter in *The Site Reliability Workbook*. <https://sre.google/workbook/eliminating-toil/> Accessed 2026-01-20.
- [7] Betsy Beyer, Niall Richard Murphy, David K. Rensin, Kent Kawahara, and Stephen Thorne. 2018. *The Site Reliability Workbook: Practical Ways to Implement SRE*. O'Reilly Media.
- [8] Panagiota Chatzipetrou, Lefteris Angelis, Paul Rovegård, and Claes Wohlin. 2010. Prioritization of Issues and Requirements by Cumulative Voting: A Compositional Data Analysis Framework. In *Proceedings of the 36th EUROMICRO Conference on Software Engineering and Advanced Applications*. 361–368. [doi:10.1109/SEAA.2010.9](https://doi.org/10.1109/SEAA.2010.9)
- [9] Panagiota Chatzipetrou, Efi Papathocharous, Lefteris Angelis, and Andreas S. Andreou. 2013. Software Effort Phase Distribution: A Statistical Framework. In *Proceedings of the 17th International Conference on Evaluation and Assessment in Software Engineering (EASE)*. 397–402. [doi:10.1145/2460999.2461054](https://doi.org/10.1145/2460999.2461054)
- [10] Panagiota Chatzipetrou, Efi Papathocharous, Lefteris Angelis, and Andreas S. Andreou. 2015. A Multivariate Statistical Framework for the Analysis of Software Effort Phase Distribution. *Information and Software Technology* 63 (2015), 1–18. [doi:10.1016/j.infsof.2014.12.017](https://doi.org/10.1016/j.infsof.2014.12.017)
- [11] Richard Cook and Jens Rasmussen. 2005. "Going Solid": A Model of System Dynamics and Consequences for Patient Safety. *Quality and Safety in Health Care* 14, 2 (2005), 130–134. [doi:10.1136/qshc.2005.015867](https://doi.org/10.1136/qshc.2005.015867)
- [12] Sidney Dekker. 2011. *Drift into Failure: From Hunting Broken Components to Understanding Complex Systems*. Routledge.
- [13] Juan José Egozcue, Jose Luis Díaz-Barrero, and Vera Pawlowsky-Glahn. 2006. Hilbert Space of Probability Density Functions Based on Aitchison Geometry. *Acta Mathematica Sinica, English Series* 22, 4 (2006), 1175–1182. [doi:10.1007/s1014-005-0768-2](https://doi.org/10.1007/s1014-005-0768-2)
- [14] Juan José Egozcue and Vera Pawlowsky-Glahn. 2005. Groups of Parts and Their Balances in Compositional Data Analysis. *Mathematical Geology* 37, 7 (2005), 795–828. [doi:10.1007/s11004-005-7381-9](https://doi.org/10.1007/s11004-005-7381-9)
- [15] Juan José Egozcue, Vera Pawlowsky-Glahn, Gloria Mateu-Figueras, and Carles Barceló-Vidal. 2003. Isometric Logratio Transformations for Compositional Data Analysis. *Mathematical Geology* 35, 3 (2003), 279–300. [doi:10.1023/A:1023818214614](https://doi.org/10.1023/A:1023818214614)
- [16] Victor Heorhiadi, Shriram Rajagopalan, Hani Jamjoom, Michael K. Reiter, and Vyas Sekar. 2016. Gremlin: Systematic Resilience Testing of Microservices. In *Proceedings of the 36th IEEE International Conference on Distributed Computing Systems (ICDCS)*. 57–66. [doi:10.1109/ICDCS.2016.11](https://doi.org/10.1109/ICDCS.2016.11)
- [17] Erik Hollnagel, David D. Woods, and Nancy Leveson (Eds.). 2006. *Resilience Engineering: Concepts and Precepts*. Ashgate. [doi:10.1201/9781315605685](https://doi.org/10.1201/9781315605685)
- [18] Anatoly A. Krasnovsky. 2026. Model Discovery and Graph Simulation: A Lightweight Gateway to Chaos Engineering. In *Proceedings of the 48th IEEE/ACM International Conference on Software Engineering: New Ideas and Emerging Results (ICSE-NIER '26)*. ACM, Rio de Janeiro, Brazil, 5. [doi:10.1145/3786582.3786823](https://doi.org/10.1145/3786582.3786823)
- [19] Nancy G. Leveson. 2011. *Engineering a Safer World: Systems Thinking Applied to Safety*. MIT Press. [doi:10.7551/mitpress/8179.001.0001](https://doi.org/10.7551/mitpress/8179.001.0001)
- [20] Bowen Li, Xin Peng, Qilin Xiang, Haolin Wang, Tao Xie, Jun Sun, and Xuanzhe Liu. 2022. Enjoy Your Observability: An Industrial Survey of Microservice Tracing and Analysis. *Empirical Software Engineering* 27, 1 (2022), 25. [doi:10.1007/s10664-021-10063-9](https://doi.org/10.1007/s10664-021-10063-9)
- [21] Josep A. Martín-Fernández, Carles Barceló-Vidal, and Vera Pawlowsky-Glahn. 2003. Dealing with Zeros and Missing Values in Compositional Data Sets Using Nonparametric Imputation. *Mathematical Geology* 35, 3 (2003), 253–278. [doi:10.1023/A:1023866030544](https://doi.org/10.1023/A:1023866030544)
- [22] Curtis Morrison and Robert Wears. 2021. Organizational Drift. In *The Nature of Patient Safety*. CRC Press. [doi:10.1201/9781003047270-10](https://doi.org/10.1201/9781003047270-10)
- [23] OpenSLO Community. 2022. OpenSLO: Open Service Level Objective Specification. <https://github.com/OpenSLO/OpenSLO> Accessed 2026-01-20.
- [24] OpenTelemetry. 2026. OpenTelemetry Specifications. <https://opentelemetry.io/docs/specs/> Accessed 2026-01-20.
- [25] Vera Pawlowsky-Glahn, Juan José Egozcue, and Raimon Tolosana-Delgado. 2015. *Modeling and Analysis of Compositional Data*. John Wiley & Sons. [doi:10.1002/9781119003144](https://doi.org/10.1002/9781119003144)
- [26] Vera Pawlowsky-Glahn, Juan José Egozcue, and K. Gerald van den Boogaart. 2014. From Compositional Data to Compositional Functions. In *Proceedings of the 1st Workshop on Functional and Operatorial Statistics*. 125–131.
- [27] Jens Rasmussen. 1997. Risk Management in a Dynamic Society: A Modelling Problem. *Safety Science* 27, 2–3 (1997), 183–213. [doi:10.1016/S0925-7535\(97\)00052-0](https://doi.org/10.1016/S0925-7535(97)00052-0)
- [28] Kaspars Rinkevics and Richard Torkar. 2013. An Empirical Study on Cumulative Voting in Software Engineering. *Information and Software Technology* 55, 4 (2013), 644–656. [doi:10.1016/j.infsof.2012.08.008](https://doi.org/10.1016/j.infsof.2012.08.008)
- [29] Benjamin H. Sigelman, Luiz André Barroso, Mike Burrows, Pat Stephenson, Manoj Plakal, Donald Beaver, Saul Jaspan, and Chandan Shanbhag. 2010. Dapper, a Large-Scale Distributed Systems Tracing Infrastructure. Technical report. <https://research.google.com/archive/papers/dapper-2010-1.pdf> Accessed 2026-01-20.
- [30] Jacopo Soldani, Javad Khalili, and Antonio Brogi. 2023. Offline Mining of Microservice-Based Architectures (Extended Version). *SN Computer Science* (2023). [doi:10.1007/s42979-023-01721-4](https://doi.org/10.1007/s42979-023-01721-4)
- [31] K. Gerald van den Boogaart and Raimon Tolosana-Delgado. 2013. *Analyzing Compositional Data with R*. Springer. [doi:10.1007/978-3-642-36809-7](https://doi.org/10.1007/978-3-642-36809-7)